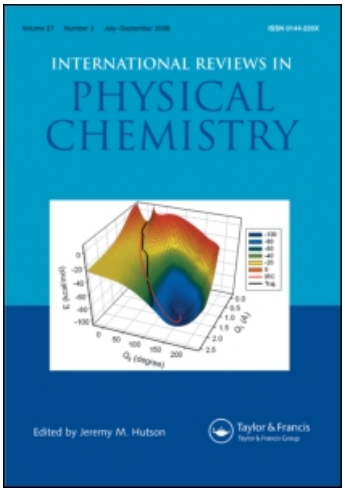

International Reviews in Physical Chemistry
Publication details, including instructions for authors and subscription information:
http://www.informaworld.com/smpp/title~content=t713724383

Linear scaling electronic structure calculations with numerical atomic basis set

Honghui Shang[a]; Hongjun Xiang[ab]; Zhenyu Li[a]; Jinlong Yang[a]
[a] Hefei National Laboratory for Physical Sciences at Microscale, University of Science and Technology of China, Hefei 230026, China [b] Key Laboratory of Computational Physical Sciences Ministry of Education) and Department of Physics, Fudan University, Shanghai 200433, China

Online publication date: 19 November 2010

To cite this Article Shang, Honghui , Xiang, Hongjun , Li, Zhenyu and Yang, Jinlong(2010) 'Linear scaling electronic structure calculations with numerical atomic basis set', International Reviews in Physical Chemistry, 29: 4, 665 — 691
To link to this Article: DOI: 10.1080/0144235X.2010.520454
URL: http://dx.doi.org/10.1080/0144235X.2010.520454

International Reviews in Physical Chemistry
Vol. 29, No. 4, October–December 2010, 665–691

Taylor & Francis
Taylor & Francis Group

Linear scaling electronic structure calculations with numerical atomic basis set

Honghui Shang[a], Hongjun Xiang[ab], Zhenyu Li[a] and Jinlong Yang[a]*

[a]*Hefei National Laboratory for Physical Sciences at Microscale, University of Science and Technology of China, Hefei 230026, China;* [b]*Key Laboratory of Computational Physical Sciences Ministry of Education) and Department of Physics, Fudan University, Shanghai 200433, China*

(*Received 27 June 2010; final version received 30 August 2010*)

We discuss in this review recent progress, especially by our group, on linear scaling algorithms for electronic structure calculations with numerical atomic basis sets. The principles of the construction of numerical basis sets and the Hamiltonian are introduced first. Then we discuss how to solve the single-electron equation self-consistently, and how to obtain electronic properties via post-self-consistent-field processes in a linear scaling way. The linear response calculation with linear scaling is also introduced. Numerical implementation is emphasized, with some applications presented for demonstration purposes.

Keywords: linear scaling algorithms; numerical atomic basis sets; electronic structure calculations; DFT; Hartree-Fock; purification algorithms; response theory

Contents

*Corresponding author. Email: jlyang@ustc.edu.cn

ISSN 0144–235X print/ISSN 1366–591X online

DOI: 10.1080/0144235X.2010.520454
http://www.informaworld.com

1. Introduction

Ab initio electronic structure calculations based on density functional theory (DFT) [1–3] or quantum-chemical approaches (Hartree–Fock theory and post-Hartree–Fock methods) [4] have been successfully applied to both molecular and condensed-matter systems. During the past few decades, with the rapid increase of computational power, it is now possible to study the electronic properties of systems containing many thousands of atoms. However, achieving a favourable scaling of the computational time with respect to the increase of system size is still essential to reach significantly larger systems in the near future.

The traditional way to calculate the ground state energy is to solve the eigenvalue equation, which has a computational cost scaling of $O(N^3)$ [5], where N is the number of atoms in the system under consideration. Such a N^3-scaling presents a serious bottleneck to deal with systems with a large number of degrees of freedom. At best, we hope the computational time increases linearly with the system size. Algorithms reaching this goal are called linear scaling or $O(N)$ algorithms.

The fundamental principle behind almost all linear scaling algorithms is Kohn's nearsightedness principle [6]. For a quantum mechanical system within an external potential $v(\mathbf{r}')$, its local properties do not see a change of the external potential if the change is limited to a distant region. This principle leads to the sparsity of the Hamiltonian matrix [5,7]. In practice, the sparsity is achieved by dropping matrix elements less than a threshold or by using strictly truncated atomic basis sets. It is demonstrated that dropping small matrix elements may cause numerical instability [8]. As a result, using strictly truncated atomic basis sets is a better choice. Analytic atomic orbitals, such as the Gaussian-type orbitals (GTOs), typically have a long tail. On the other hand, numerical atomic orbitals (NAOs) can be strictly truncated by applying a confining potential.

There are numerous NAO-based DFT implementations [8–19] in the local density approximation (LDA) or generalized gradient approximation (GGA). An NAO basis set has also been implemented in Hartree–Fock calculations for molecular systems [20–26]. Using the locality of NAO, various $O(N)$ algorithms have been proposed to deal with systems containing thousands of atoms [8,27–33]. In the present paper, we focus on $O(N)$ numerical algorithms to calculate electronic structures of molecules and periodic systems.

The outline of this review is as follows. The discussion begins with the construction of NAOs (Section 2), which are typically the product of a numerical radial function and a spherical harmonic. The ways to generate radial functions can be divided into two categories: the all-electron methods and pseudopotential methods. With an NAO basis set ready, the first task for a DFT calculation is the construction of the Hamiltonian

matrix (Section 3), which typically involves real-space grid operations or Fourier space operations for two-centre integrals. Since the Hamiltonian depends on the charge density, the single-electron problem needs to be solved self-consistently. There have been numerous $O(N)$ algorithms developed to update the density matrix in the self-consistent field (SCF) cycles. In Section 4, we introduce several representative ones, including the trace-correcting scheme and the trace-resetting scheme. Besides a linear scaling SCF, it is also desirable to have $O(N)$ scaling for other post-SCF tasks in electronic structure calculations, such as the calculation of the energy gap between the highest occupied molecular orbital (HOMO) and the lowest unoccupied molecular orbital (LUMO) and the construction of localized orbitals. A detailed description of this kind of method to obtain properties beyond the total energy is given in Section 5. In Section 6, we discuss the response theory based on the locality of the density matrix, i.e. linear scaling density matrix perturbation theory (DMPT) [34]. Section 7 concludes the review.

2. Numerical atomic orbitals

At the very beginning, NAOs were developed to calculate electronic structure for atoms [35]. Then, it is found that the one-particle wavefunctions of molecules can be well described by linear combinations of numerical atomic orbitals (LCAO). In the chemistry community, the use of atomic orbitals, e.g. GTOs [36–41], is very popular. In solid-state physics, LCAOs have also been regarded as an efficient approach to extend the applicability of DFT to realistic large systems. For example, Sankey and Niklewski [9] have used the slightly excited pseudo-atomic-orbitals to derive the tight-binding Hamiltonian matrix in real space. In the last few decades, great efforts have been made to construct efficient and accurate localized orbitals [13,17,18,42,43] as a basis set in $O(N)$ calculations.

An NAO for atom I, located at R_I is the product of a numerical radial function and a spherical harmonic:

$$\phi_{Ilmn}(\mathbf{r}) = \varphi_{Iln}(r_I)\mathbf{Y}_{lm}(\hat{r_I}) \tag{1}$$

where $r_I = r - R_I$, and the index n denotes the orbitals with the same angular dependence, but different radial dependence. l is the orbital angular momentum quantum number, and m is the magnetic quantum number.

The radial part of the numerical atomic orbital $\varphi_{Iln}(r)$ is calculated by the following equation:

$$\left(-\frac{1}{2}\frac{\mathrm{d}^2}{\mathrm{d}r^2}r + \frac{l(l+1)}{2r^2} + V_l(r) + V_{\mathrm{cut}}\right)\varphi_{Iln}(r) = \epsilon_l\varphi_{Iln}(r) \tag{2}$$

where $V_l(r)$ denotes the electrostatic potential for orbital $\varphi_{Iln}(r)$, and V_{cut} ensures a smooth decay of each radial function to be strictly zero outside a confining radius r_{cut}.

There are many kinds of methods to construct radial NAOs. For example, SIESTA [8] uses an energy shift to apply different spherical confinements in its minimal basis set, following Sankey and Niklewski [9], then splits the norm for multiple-zeta, and constructs the polarization part by applying an electric field; FHI-AIM [33] uses a smooth analytical shape potential to get a minimal basis set, and then additional NAO basis functions are

constructed by optimizing from a large pool of 'candidate' radial functions; OpenMX [32,44,45] uses the eigenstates of an atomic Kohn–Sham equation with a confinement pseudopotential as the primitive orbitals, and then variationally optimizes the NAOs of each atom in a given system based on the force theorem; and DMOL^3 [19,46] uses exact LDA spherical-atom orbitals in the basis set. We categorize them into two classes: all-electron NAOs and pseudopotential NAOs. In the following, we will use FHI-AIM and SIESTA as two examples to describe them.

2.1. *All-electron numerical atomic orbitals*

In all-electron NAOs, a confining potential is used to get the localized orbitals. Two kinds of confining potential have been discussed by several authors, i.e. the simplest 'hard-wall' potential as used by Sankey and Niklewski [9], and smooth analytical shape potentials [43,47]. In the FHI-AIM framework [33,48], the following smooth analytical potential is used:

$$V_{\mathrm{cut}}(r) = \begin{cases} 0 & r \le r_{\mathrm{onset}} \\ s \cdot \exp\left(\dfrac{w}{r - r_{\mathrm{onset}}}\right) \cdot \dfrac{1}{(r - r_{\mathrm{cut}})^2} & r_{\mathrm{onset}} < r < r_{\mathrm{cut}} \\ \infty & r \ge r_{\mathrm{cut}} \end{cases} \tag{3}$$

where the parameters are set as $s = 200$ Hartree and $w = 2.0$ Å. The suggested value for r_{onset} is 3.5 Å for light elements and 4.0 Å for transition metals. The confinement potential V_{cut} and its impact on the tails of an atomic Au 6*s* radial function and its second derivative are illustrated in Figure 1.

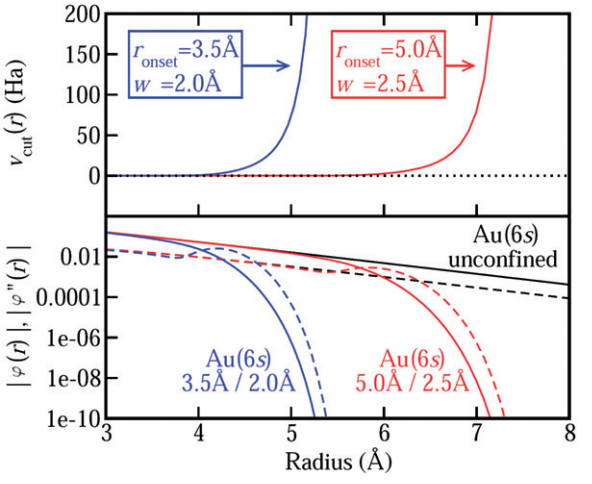

Figure 1. [Colour online] The Au 6*s* radial function generated with different confining potentials $V_{\mathrm{cut}}(r)$ by FHI-AIM. Upper panel: Basis set confining potentials $V_{\mathrm{cut}}(r)$ as defined in Equation (3), for two different settings of r_{onset} and w ($s = 200$ Hartree in both cases). Lower panel: Influence of $V_{\mathrm{cut}}(r)$ on the tails of the Au 6*s* radial function $\varphi(r)$ (solid lines) and its second derivative $\varphi''(r)$ (dashed lines) for both settings, compared to the unconfined case. (Reproduced with permission from ref. [33]. Copyright 2009 Elsevier.)

The minimal basis set that consists of the core and valence functions of an atom can be calculated by solving Equation (2) with $V_l(r)$ set to the free-atom radial potential. The radial equations are solved in one dimension on a logarithmic radial grid, and the radial functions so obtained are then orthonormalized by a simple Gram–Schmidt procedure. A cubic spline interpolation is finally used to smooth the radial functions.

After the minimal basis set is ready, additional NAO basis functions are constructed at different levels by the following strategy: (1) Define a large pool of 'candidate' radial functions, including the radial functions of doubly positively charged free ions and hydrogen-like radial functions for a potential z/r with z in the range $0.1 \le z \le 20$. (2) Starting from the minimal basis set, each function in the pool of candidate functions is added in turn; the radial function that gives the single largest improvement of a target total energy is added to the original basis set. (3) The procedure is repeated until there is no further significant total energy improvement.

With the optimization procedure described above, different tiers of basis sets can be obtained for different levels of calculations.

2.2. *Pseudopotential numerical atomic orbitals*

Pseudo-atomic orbitals (PAOs) can be obtained in several ways. Here we focus on SIESTA's recipe since it is efficient and popular [42]. If a pseudopotential is used to describe the ion–electron interaction in an atom, this atom is called a pseudo-atom. There are two ways to construct the minimal (single-ζ) basis set in SIESTA. One is using the eigenfunctions of a pseudo-atom within a spherical box, i.e. the simplest 'hard-wall' potential is used as the confining potential. In this way, a single parameter (ΔE_{PAO}) that describes the energy increase due to the confinement of the finite sphere can be used to define the radii of different orbitals. It is found that a ΔE_{PAO} between 100 and 200 meV typically leads to precision within the accuracy of current DFT functionals. The other way [43] is to use a soft confinement potential [49,50] as:

$$V_{\mathrm{cut}}(r) = V_{\mathrm{o}} \frac{e^{-(r_c - r_i)/(r - r_i)}}{r_c - r} \tag{4}$$

where r_i is the inner radius where the soft confinement potential starts off, and r_c is the cutoff radius to ensure strict localization there. V_{o} is the prefactor of this soft confinement potential. These parameters are optimized variationally to minimize the systems' total energy.

To obtain multiple-ζ basis sets, the best scheme so far is to add a numerical orbital which has the same tail as the first-ζ orbital, $\phi_l^{1\zeta}(r)$, and continues smoothly towards the origin as $r^l(a_l - b_l r^2)$ inside a 'split radius' r_l^s, i.e.

$$\phi_l^{2\zeta}(r) = \begin{cases} r^l(a_l - b_l r^2) & r < r_l^s \\ \phi_l^{1\zeta}(r) & r \ge r_l^s \end{cases} \tag{5}$$

where r_l^s is determined by fixing the norm of $\phi_l^{1\zeta}(r)$ in $r \ge r_l^s$; it is found that 0.15 is a reasonable value for the 'norm'. Then a_l and b_l are obtained by ensuring continuity and differentiability at r_l^s. In practice, the $\phi_l^{1\zeta} - \phi_l^{2\zeta}$ orbital is used to reduce the number of

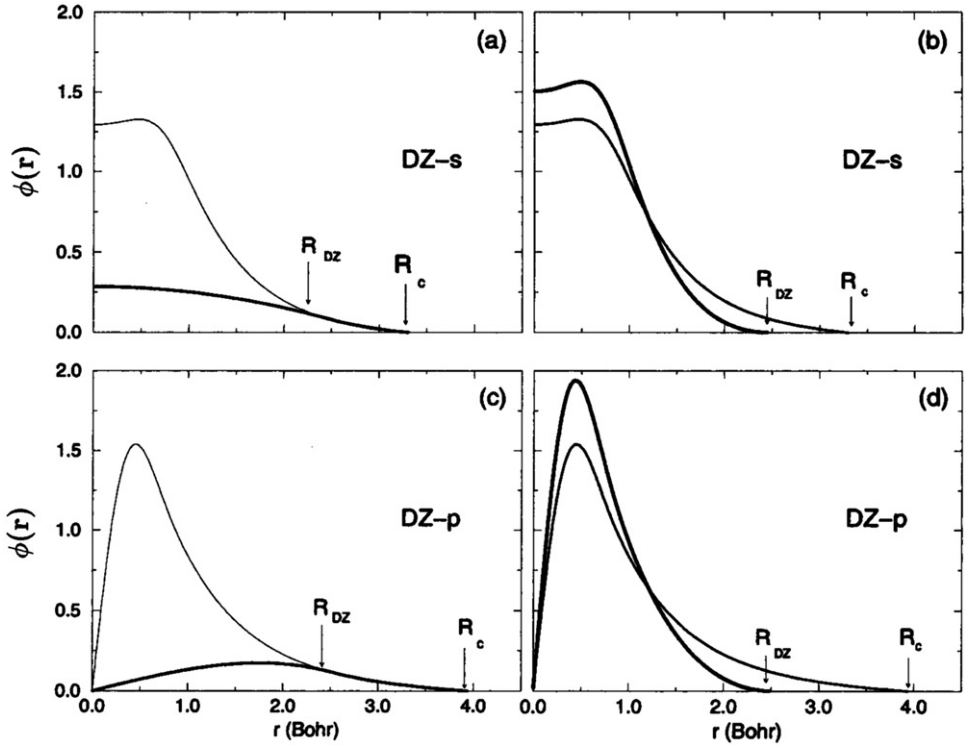

Figure 2. Confined pseudo-atomic orbitals for oxygen: (a) and (b) for *s* orbital, and (c) and (d) for *p* orbital. R_c is the confinement radius obtained with $\Delta E_{\mathrm{PAO}} = 250\,\mathrm{meV}$. The original PAOs ($\phi_l^{1\zeta}$) are represented with thinner lines. The split smooth functions ($\phi_l^{2\zeta}$) are plotted with thicker lines in (a) and (c), while the resulting double-ζ orbitals ($\phi_l^{1\zeta} - \phi_l^{2\zeta}$) are plotted with thicker lines in (b) and (d). (Reproduced with permission from ref. [42]. Copyright 1999 Wiley.)

non-zero matrix elements in the same Hilbert space. In Figure 2, the double-ζ PAOs for oxygen are plotted.

Polarization orbitals are those with an angular momentum $l+1$ to describe the polarization of valence orbitals with an angular moment l. In SIESTA, the polarization orbitals are obtained by an actual polarization of the pseudo-atom with a small electric field. The $l+1$ orbital can then be exactly solved through comparison with first-order perturbation theory. Based on exhaustive tests, the double-ζ plus polarization (DZP) basis set has proved to be a basis set that can yield accurate results in most cases.

To demonstrate the efficiency of the SIESTA basis set, the energy differences per atom compared with a converged plane-wave result were calculated using both LDA and GGA functionals for two amino acids: glycine and alanine. Two different methods were used to generate NAO basis sets: the SIESTA PAOs, up to DZP, and increasing eigenstates, up to TZTP. It turns out that the SIESTA basis sets are more efficient than the atomic eigenstates (Figure 3).

Recently, the SIESTA group proposed a method to control, in-depth, the range of the basis sets by a single parameter [47] that allows us to monitor their convergence with the range of basis sets in a simple and systematic way.

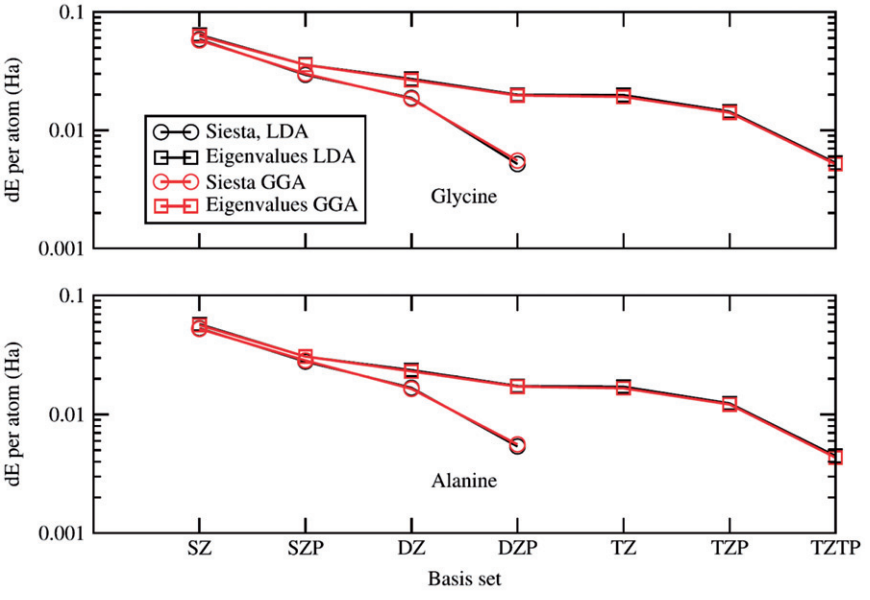

Figure 3. [Colour online] Convergence with basis sets of SIESTA PAOs and eigenvalue-based PAOs for glycine (top) and alanine (bottom). Energy differences per atom are relative to the converged plane-wave result. (Reproduced with permission from ref. [27]. Copyright 2008 Institute of Physics.)

3. Building the Hamiltonian

In mean field theories of electronic structure theory, there are two computationally demanding tasks [51–53]: construction of the single-electron Hamiltonian (the Fock matrix), which conventionally scales quadratically with molecular size [54], and updating the density matrix, which is conventionally done by diagonalization, scaling cubically with system size. The latter shows a very small prefactor and therefore it only becomes important for very large systems. The construction of the Fock matrix involves two computationally expensive parts: Coulomb and exchange terms.

For the Coulomb problem, there have been various effective linear scaling methods introduced based on GTOs [55–60], such as the fast multipole method (FMM). With NAO basis sets, the Coulomb term is calculated on a real-space grid [8], and this allows good scaling with growing system size.

The exchange term is a functional of the density in DFT. But the computation of electron repulsion integrals is required in Hartree–Fock theory and hybrid DFT methods, such as in the popular B3LYP functional [61]. With the GTO basis set, several approaches to reduce the computational scaling property of exact exchange evaluation have been introduced [54,62–64]. For example, the ONX (order-N exchange) algorithm by Schwegler *et al*. [64] employs traditional SCF density-weighted integral estimations of exchange within a novel loop structure and LinK (Linear exchange K) method [54] based on ONX exploits the full permutational symmetry of the two-electron integrals. With NAOs, the exchange term is more difficult to obtain [33,65,66]. In this section, we focus on our linear scaling implementation in SIESTA [67].

3.1. *Kohn–Sham DFT Hamiltonian*

In the Kohn–Sham DFT scheme, the Hamiltonian can be written as:

$$H = T + \sum_I V_I^{\mathrm{KB}} + \sum_I V_I^{\mathrm{local}}(r) + V^{\mathrm{H}}(r) + V^{\mathrm{XC}}(r) \tag{6}$$

where T is the kinetic energy operator, I is the atom index, $V_I^{\mathrm{local}}(r)$ and V_I^{KB} are the local and non-local parts [68] of the pseudopotential on atom I, V^{H} is the Hartree potential operator, and V^{XC} is the exchange-correlation potential operator, which is local in pure DFT, but is non-local in HF. In the SIESTA implementation, the Hamiltonian is rewritten as:

$$H = T + \sum_I V_I^{\mathrm{KB}} + \sum_I V_I^{\mathrm{NA}}(r) + \delta V^{\mathrm{H}}(r) + V^{\mathrm{XC}}(r) \tag{7}$$

where the long-range local part of the pseudopotential is combined with the neutral-atom potential, forming a screened 'neutral-atom' (NA) potential, $V_I^{\mathrm{NA}} \equiv V_I^{\mathrm{local}} + V_I^{\mathrm{atom}}$, and $\delta V^{\mathrm{H}}(r)$ is the electrostatic potential generated by $\delta\rho(r)$ which is equal to $\rho(r) - \sum_I \rho_I^{\mathrm{atom}}$, usually much smaller than $\rho(r)$. In this Hamiltonian form, different terms are treated based on the type of integrals. The first two terms are two-centre integrals. They can be calculated in reciprocal space. After taking the Fourier transform, the kinetic matrix and the non-local psodopotential elements can be written in the following form:

$$T_{\mu\nu} = \int k^2 \psi_\mu^*(k)\psi_\nu(k)\mathrm{e}^{-ikR}\mathrm{d}k \tag{8}$$

$$V_{\mu\nu}^{\mathrm{KB}} = \sum_\alpha \int \psi_\mu^*(k)\chi_\alpha(k)\mathrm{e}^{-ikR_1}\mathrm{d}k v_\alpha^{\mathrm{KB}} \int \chi_\alpha(k)^*\psi_\nu(k)\mathrm{e}^{-ikR_2}\mathrm{d}k \tag{9}$$

where $\psi_\mu(k)$ and $\psi_\nu(k)$ are basis functions in their Fourier space, $\chi_\alpha(k)$ is KB projector in its Fourier space, and α denotes all the KB projectors that overlap with ψ_μ and ψ_ν. With localized numerical atomic orbitals, the maximum number of each atom's neighbour is constant, so two-centre integration can be performed in an $O(N)$ operation.

The remaining three terms are three-centre integrals, which are calculated on a real-space grid. V_I^{NA} is tabulated as a function of distance to atom I, and it can be evaluated at any desired grid point by interpolation. $\delta V^{\mathrm{H}}(r)$ is calculated by solving Poisson's equation. The last term, $V^{\mathrm{XC}}(r)$, can be easily calculated in pure density functional forms. Therefore, for functionals without exact exchange, we have the total grid potential $V(r) = V^{\mathrm{NA}} + \delta V^{\mathrm{H}}(r) + V^{\mathrm{XC}}(r)$. At every grid point, $V(r)\psi_\mu^*\psi_\nu\Delta v$ can be calculated for the orbital pair (ψ_μ^*, ψ_ν) which is not zero at that point (Δv is the volume per grid point). It is then added to the Hamiltonian matrix element $H_{\mu\nu}$.

3.2. *Hartree–Fock type exchange*

The widely used functionals based on LDA or GGA are sometimes not accurate enough [69]. A possible remedy is adding non-local Hartree–Fock type exchange (HFX) into local or semi-local density functionals. We have presented an accurate strategy for the efficient HFX calculation in real-space with localized NAO basis sets implemented in the SIESTA

$$(\chi_\mu^{\mathbf{0}}\chi_\nu^{\mathbf{N}}|\chi_\lambda^{\mathbf{G}}\chi_\sigma^{\mathbf{H}}) = \int\int \frac{\chi_\mu^{\mathbf{0}}(\mathbf{r})\chi_\nu^{\mathbf{N}}(\mathbf{r})\chi_\lambda^{\mathbf{G}}(\mathbf{r}')\chi_\sigma^{\mathbf{H}}(\mathbf{r}')}{|\mathbf{r}-\mathbf{r}'|}\mathbf{dr}\mathbf{dr}'$$

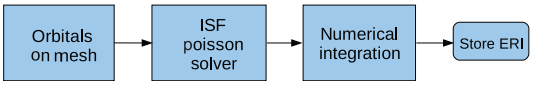

Figure 4. [Colour online] The scheme to calculate ERIs within NAOs. (Reproduced with permission from ref. [67]. Copyright 2010 American Chemical Society.)

package [67]. In LDA and GGA, $V^{\mathrm{XC}}(r)$ is the same in every unit cell. However, in the HFX case, $V^{\mathrm{XC}}(r, r')$ is non-local, and the HFX potential matrix element is defined as

$$[V^{\mathrm{X}}]_{\mu\lambda}^{\mathbf{Q}} = -\frac{1}{2}\sum_{\nu\sigma}\sum_{\mathbf{N}}\rho_{\nu\sigma}^{\mathbf{N}}\sum_{\mathbf{H}}[(\chi_\mu^{\mathbf{0}}\chi_\nu^{\mathrm{H}}|\chi_\lambda^{\mathrm{Q}}\chi_\sigma^{\mathrm{H+N}})] \tag{10}$$

where **Q**, **H**, and **N** represent different unit cells, and summations of **H** and **N** run for all unit cells in the extended cell. The density matrix element $\rho_{\nu\sigma}^{\mathbf{N}}$ is computed by an integration over the Brillouin zone (BZ)

$$\rho_{\nu\sigma}^{\mathbf{N}} = \sum_j \int_{\mathrm{BZ}} c_{\nu,j}^*(\mathbf{k})c_{\sigma,j}(\mathbf{k})\theta(\epsilon_F - \epsilon_j(\mathbf{k}))\mathbf{e}^{i\mathbf{k}\cdot\mathbf{N}}\mathbf{dk} \tag{11}$$

where θ is the step function, ϵ_F is the Fermi energy and $\epsilon_j(\mathbf{k})$ is the j-th eigenvalue at point **k**.

In order to calculate the electron repulsion integrals (ERIs) in Equation (10) in a real-space grid, we first calculate

$$\mathbf{V}_{\mu^{\mathbf{0}},\nu^{\mathbf{N}}}(\mathbf{r}') = \int \frac{\chi_\mu^{\mathbf{0}}(\mathbf{r})\chi_\nu^{\mathbf{N}}(\mathbf{r})}{|\mathbf{r}-\mathbf{r}'|}\mathrm{d}\mathbf{r} \tag{12}$$

which is obtained by solving Poisson's equation in real space with free boundary condition, using the interpolating scaling functions (ISF) method [70]. The next step is an integration also in real space

$$(\chi_\mu^{\mathbf{0}}\chi_\nu^{\mathbf{N}}|\chi_\lambda^{\mathbf{Q}}\chi_\sigma^{\mathbf{H}}) = \int \mathbf{V}_{\mu^{\mathbf{0}},\nu^{\mathbf{N}}}(\mathbf{r}')\chi_\lambda^{\mathbf{Q}}(\mathbf{r}')\chi_\sigma^{\mathbf{H}}(\mathbf{r}')\mathrm{d}\mathbf{r}'. \tag{13}$$

The whole scheme is summarized in Figure 4.

We have studied the one-dimensional polymer *trans*-polyacetylene as a benchmark for extended systems. We optimize its geometry with CRYSTAL 06, using a B3LYP functional and 6-31G** basis set. With this optimized geometry, we calculate its band structure. The single-zeta (SZ), double-zeta (DZ), and double-zeta plus polarization (DZP) basis sets are employed with our code and the STO-3G, 6-31G, and 6-31G** basis sets are employed with CRYSTAL 06. We sampled the Brillouin zone by $1 \times 1 \times 200$ special k-points using the Monkhorst–Pack scheme. The five highest occupied bands, along with the three lowest conduction bands, are plotted in Figure 5. We can see that the agreement between the numerical and analytical basis sets is good. The CRYSTAL 06 band structure has been rigidly shifted to make the valence band edges coincide when compared with our

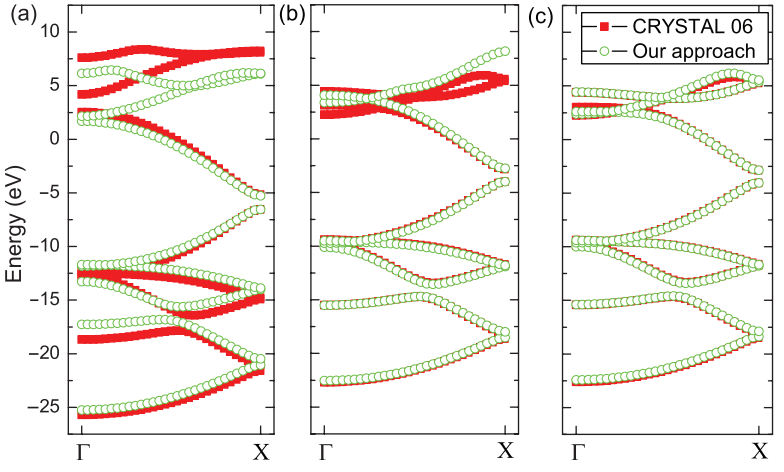

Figure 5. [Colour online] Band structure of *trans*-polyacetylene calculated with the B3LYP functional using (a) SZ, (b) DZ, and (c) DZP basis sets. (Reproduced with permission from ref. [67]. Copyright 2010 American Chemical Society.)

result, since the absolute values of the band energies are generally different for different approaches owing to the different treatment of the Coulomb series. A bigger basis set leads to better agreement between our results with those obtained with a Gaussian basis set in the CRYSTAL 06 package.

4. Linear scaling construction of the density matrix

After the Hamilton matrix is built, the density matrix can be obtained by diagonalizing the Hamilton matrix, which has a computational cost scaling of $O(N^3)$. In 1991, Yang [71] proposed a linear scaling method for this purpose. Now there have been many different approaches for $O(N)$ electronic structure calculations. Below we briefly review three types of $O(N)$ algorithms: direct methods, variational methods, and purification methods. The detailed description and comparison of the first two classes of methods can be found in Goedecker's review [5]. The last one tends to be more efficient when implemented with NAOs [72–74] and it will be described in more detail in this review.

4.1. *Direct methods*

The direct approaches are featured by direct calculation of density matrix elements using various approximations, which include the divide-and-conquer (DC) method [71,75,76], the Fermi operator expansion (FOE) method [77–79], and the kernel polynomial method (KPM) [80].

In the DC method proposed by Yang [71], a system is divided into disjoint subsystems. Then the truncation of the density matrix is applied, which leads to a linear scaling calculation of the band structures.

At a finite temperature, the density operator can be expressed as a Fermi–Dirac distribution function of the Hamiltonian. The Fermi–Dirac distribution $f(H)$ can then be approximated by a polynomial function of H, such as a Chebyshev polynomial representation. Therefore, only sparse matrix multiplications are required to get the new density matrix, which scales linearly [78,79].

The kernel polynomial method, developed by Voter and coworkers [80], is to convolute the density of states (DOS) and the step function with the kernel polynomial, which is similar in concept to the FOE method.

4.2. *Variational methods*

The second class of $O(N)$ methods is based on variational approaches, including the density matrix minimization (DMM) method [81–83], the penalty function-based energy minimization approach [7,84], variational approaches using localized orbitals minimization (LOM) [85–88], and the absolute energy minimum approach [89].

In 1993, Li, Nunes, and Vanderbilt (LNV) proposed an algorithm to minimize the grand potential $\Omega = 2\mathrm{Tr}[(3\rho^2 - 2\rho^2)(H - \mu)]$ instead of minimizing the energy E directly, where ρ is the density matrix. The grand potential includes McWeeny's purification transformation [90] to impose the idempotency constraint ($\rho^2 = \rho$). Then the conjugate-gradient method is used to minimize the DMM functional. This method is based on a variational solution for the density matrix, which is truncated to zero beyond a real-space radius, so the computational time scales linearly with system size. The DMM method has been successfully implemented for orthogonal tight-binding Hamiltonians [81].

The CONQUEST group [91–99] has implemented the LNV scheme into DFT calculations. They express $\rho(r, r')$ as

$$\rho(r, r') = \sum_{i\alpha, j\beta} \phi_{i\alpha}(r) K_{i\alpha, j\beta} \phi_{j\beta}(r') \tag{14}$$

where $\phi_{i\alpha}(r)$ is a support function for atom i, and the multiple support functions on the same atom are labelled with α. The support functions can be represented in terms of either the quantitative basis set using blip functions or smaller sized NAOs for which systematic convergence is usually significantly harder. $K_{i\alpha, j\beta}$ is the density matrix in the basis of support functions. The support functions are non-orthogonal, and the associated overlap matrix is:

$$S_{i\alpha, j\beta} = \int \mathrm{d}\mathbf{r}\, \phi_{i\alpha}(\mathbf{r}) \phi_{j\beta}(\mathbf{r}). \tag{15}$$

K can be written in terms of an auxiliary density matrix L,

$$K = 3LSL - 2LSLSL \tag{16}$$

to achieve idempotency. The ground state is obtained by minimizing the total energy with respect to support functions and to the auxiliary density matrix (L) under the constraint of a fixed number of electrons. Using their extensively optimized sparse matrix multiplication algorithm [100], the CONQUEST method has demonstrated the possibility of DFT calculations to treat millions of atoms [91].

Kohn [7] and later Haynes and Payne [84] have imposed the condition of idempotency of the density matrix by a penalty function and then used the variational scheme to determine the density matrix by energy minimization.

Mauri *et al.* [85,86] used an unconstrained variational approach to minimize the energy functional with respect to the set of localized orbitals, and this leads to an approximate ground state energy. Ordejón *et al.* [87,101] also proposed an unconstrained minimization scheme by introducing an energy functional,

$$E = 2\left[\sum_{i=1}^{N} H_{ii} - \sum_{i,j=1}^{N} (S_{ij} - \delta_{ij})H_{ji}\right] \tag{17}$$

and then the conjugate gradient scheme can be used to minimize the energy functional. The calculation of the energy functional scales linearly with system size by introducing truncated Wannier-like wavefunctions. But this scheme suffers from the problem of multiple local minima in numerical calculations [101].

4.3. *The purification methods*

The third class of $O(N)$ algorithm is purification methods, including the trace-preserving canonical purification scheme of Palser and Manolopoulos (PM) [102], trace-correcting purification (TC) [73], and the trace resetting density matrix purification approach (TRS) [72]. All the purification algorithms described above do not need the input of the chemical potential, and they are very efficient when no prior knowledge of the chemical potential is available [5,72,73,103,104].

The first purification algorithm for density matrix construction was proposed by Palser and Manolopoulos [102]. This method works with a predefined occupation and does not need the input or adjustment of the chemical potential. They start with an estimated initial density matrix, ρ_0, which has a trace equal to the occupation number. Then, trace-conserving spectral projections are performed, until the density matrix ρ_n converges to the correct density matrix. The canonical PM scheme is given in pseudocode Algorithm 1.

Algorithm 1: The PM algorithm, where N_e is the number of electrons, N_b denotes the number of basis sets, $\varepsilon_{\min}(H)$ denotes the minimal eigenvalue of the Hamiltonian matrix H, and $\varepsilon_{\max}(H)$ denotes the maximum eigenvalue of the Hamiltonian matrix H.

subroutine PM(H, ρ, N_e, N_b)
estimate $\varepsilon_{\min}(H)$, $\varepsilon_{\max}(H)$
$\alpha = \frac{1}{N_b}\min(\frac{N_e}{\varepsilon_{\max}-\mu}, \frac{N_b-N_e}{\mu-\varepsilon_{\min}})$
$\beta = N_e/N_b$, $\mu = \mathrm{Tr}[H]/N_b$
$\rho_0 = \alpha(\mu I - H) + \beta I$
while *Error* > *ErrorLimit* **do**
  $c_n = \frac{\mathrm{Tr}[\rho_n^2-\rho_n^3]}{\mathrm{Tr}[\rho_n-\rho_n^2]}$
  if $c_n \geq 1/2$ **then**
    $\rho_{n+1} = \frac{(1+c_n)\rho_n^2-\rho_n^3}{c_n}$

else
$\rho_{n+1} = \frac{(1-2c_n)\rho_n + (1+c_n)\rho_n^2 - \rho_n^3}{1-c_n}$
end
estimate Error
end
$\rho = \rho_n$

The PM scheme performs excellently compared with DMM methods [74,102]. However, the method is inefficient at low and high partial occupancies. As a result, Niklasson [73] proposed the TC algorithm. Its second-order form is called the second-order trace-correcting purification (TC2) method:

$$\rho_{n+1}(\rho_n) = \begin{cases} \rho_n^2 & \mathrm{Tr}(\rho_n \geq N_e) \\ 2\rho_n - \rho_n^2 & \mathrm{Tr}(\rho_n < N_e). \end{cases} \tag{18}$$

The TC2 scheme is described in pseudocode Algorithm 2.

Algorithm 2: The TC2 algorithm, where N_e is the number of electrons, $\varepsilon_{\min}(H)$ denotes the minimal eigenvalue of the Hamiltonian matrix H, and $\varepsilon_{\max}(H)$ denotes the maximum eigenvalue of the Hamiltonian matrix H.

subroutine TC2(H, ρ, N_e)
estimate $\varepsilon_{\min}(H)$, $\varepsilon_{\max}(H)$
$\rho_0 = (\varepsilon_{\max} I - H)/(\varepsilon_{\max} - \varepsilon_{\min})$
while *Error* > *ErrorLimit* **do**
if $\mathrm{Tr}[\rho_n] - N_e < 0$ **then**
$\rho_{n+1} = 2\rho_n - \rho_n^2$
else
$\rho_{n+1} = \rho_n^2$
end
estimate Error
end
$\rho = \rho_n$

The TC2 method has an improved performance for systems with high or low filling; however, the TC2 method does not have the ability to deal with degeneracy and fractional occupancy. As a result, Niklasson [72] then developed the TRS method, and its fourth-order form (TRS4) is described by Algorithm 3.

Algorithm 3: The TRS4 algorithm, where N_e is the number of electrons, $\gamma_{\min}$ is 0, and $\gamma_{\max}$ is 6, $F(x) = x^2(4x - 3x^2)$, $G(x) = x^2(1-x)^2$, $\varepsilon_{\min}(H)$ denotes the minimal eigenvalue of the Hamiltonian matrix H, and $\varepsilon_{\max}(H)$ denotes the maximum eigenvalue of the Hamiltonian matrix H.

subroutine TRS4(H, ρ, N_e)
estimate $\varepsilon_{\min}(H)$, $\varepsilon_{\max}(H)$
$\rho_0 = (\varepsilon_{\max} I - H)/(\varepsilon_{\max} - \varepsilon_{\min})$
while *Error* > *ErrorLimit* **do**
$\gamma_n = \frac{N_e - \mathrm{Tr}[F(\rho_n)]}{\mathrm{Tr}[G(\rho_n)]}$

if $\gamma_n > \gamma_{\max}$ **then**
$\rho_{n+1} = 2\rho_n - \rho_n^2$
else if $\gamma_n < \gamma_{\min}$ **then**
$\rho_{n+1} = \rho_n^2$
else
$\rho_{n+1} = F(\rho_n) + \gamma_n G(\rho_n)$
end
estimate Error
end
$\rho = \rho_n$

We recently proposed some linear scaling methods to deal with magnetic systems. We found that the TC2 scheme can be extended to the spin polarized case simply by calculating the alpha and beta electrons separately. We denote this method as PSUTC2, and such a method needs the predetermined spin multiplicity. For magnetic systems without knowledge on their spin multiplicity, we developed the spin-unrestricted TC2 (SUTC2) method [28].

Algorithm 4: The SUTC2 algorithm, where N_e is the number of electrons, $\varepsilon_{\min}(H)$ denotes the minimal eigenvalue of the Hamiltonian matrix H, and $\varepsilon_{\max}(H)$ denotes the maximum eigenvalue of the Hamiltonian matrix H. (From [28].)

subroutine SUTC2(H_α, H_β, ρ_α, ρ_β, N_e)
estimate $\varepsilon_{\min}(H_\alpha)$, $\varepsilon_{\max}(H_\alpha)$, $\varepsilon_{\min}(H_\beta)$, $\varepsilon_{\max}(H_\beta)$
$\varepsilon_{\max} = \max(\varepsilon_{\max}(H_\alpha), \varepsilon_{\max}(H_\beta))$
$\varepsilon_{\min} = \min(\varepsilon_{\min}(H_\alpha), \varepsilon_{\min}(H_\beta))$
$\rho_{\alpha,0} = (\varepsilon_{\max} I - H_\alpha)/(\varepsilon_{\max} - \varepsilon_{\min})$
$\rho_{\beta,0} = (\varepsilon_{\max} I - H_\beta)/(\varepsilon_{\max} - \varepsilon_{\min})$
while *Error* > *ErrorLimit* **do**
if $\mathrm{Tr}[\rho_{\alpha,n} + \rho_{\alpha,n}] - N_e < 0$ **then**
$\rho_{\alpha,n+1} = 2\rho_{\alpha,n} - \rho_{\alpha,n}^2$
$\rho_{\beta,n+1} = 2\rho_{\beta,n} - \rho_{\beta,n}^2$
else
$\rho_{\alpha,n+1} = \rho_{\alpha,n}^2$
$\rho_{\beta,n+1} = \rho_{\beta,n}^2$
estimate Error
end
$\rho_\alpha = \rho_{\alpha,n}$
$\rho_\beta = \rho_{\beta,n}$

In the SUTC2 method, we first get the initial density matrices $\rho_{\alpha,0}$ and $\rho_{\beta,0}$ with all their eigenvalues in the range $[0, 1]$. Then $\rho_{\alpha,n}$ and $\rho_{\beta,n}$ are updated based on the sum of the traces. According to the Aufbau principle, the monotonicity of the purification polynomial leads to the correct occupations. The SUTC2 algorithm is listed in Algorithm 4.

In the implementation of purification algorithms, the key to a linear scaling is the use of sparse matrix operations. Saravanan *et al.* [105] showed that the multi-atom-blocked sparse matrix multiplications can be much faster than a standard element-by-element

sparse matrix package and also more efficient than atom-blocked sparse matrix algebra. The blocking scheme benefits from the use of highly optimized level-three basic linear algebra subroutines (BLAS) for large submatrix multiplications. So the blocked compressed sparse row (BCSR) [105–107] data structure with multi-atom blocks is very efficient for sparse matrix computations.

The BN(5, 5) nanotube with a boron atom substituted by a carbon has been chosen as a test case. Both the PSUTC2 and SUTC2 methods were tested and found to work well. With the PSUTC2 method, the magnetic moment of this system is fixed to $1\mu_B$ [108]. As shown in Figure 6, the PSUTC2 method is 25% faster than the SUTC2 method.

Although there are no unfilled shells in spin-unrestricted HF theory, as proved by Bach *et al.* [109], for spin-unrestricted DFT methods, sometimes fractional occupation is possible. In these cases PM [102] or fourth-order trace resetting (TRS4) [72] purification can be extended to the spin-unrestricted form in a similar way as in SUTC2.

5. Beyond the total energy

After the SCF process, we may want to get information about canonical or localized orbitals. It is very desirable to get such electronic properties beyond the total energy also in linear scales. Below we focus on $O(N)$ calculations of frontier molecular orbitals and maximally localized Wannier functions (MLWFs).

5.1. *O(N) calculation of band edge states and doped semiconductors*

Many linear scaling methods can only give the density matrix or the localized Wannier functions, and cannot provide the canonical wavefunctions and corresponding eigenvalues. Those states near the Fermi level are often of special interest. As a result, we have developed an $O(N)$ method to deal with the band edge states using the Lanczos method [31]. For a closed-shell system, in the canonical molecular orbital representation, the density matrix ρ and Hamiltonian H are diagonal matrices of the following forms:

$$\rho = \mathrm{diag}(1, 1, \ldots, 1, 0, 0, \ldots, 0), \quad H = \mathrm{diag}(\epsilon_1, \epsilon_2, \ldots, \epsilon_{N_e/2}, \epsilon_{N_e/2+1}, \ldots, \epsilon_{N_b}) \tag{19}$$

where N_e is the number of electrons of this system and N_b is the number of basis functions. Without loss of generality, the order of ϵ can be assumed to be:

$$\epsilon_1 \leqslant \epsilon_2 \leqslant \cdots \leqslant \epsilon_{N_e/2} \leqslant \epsilon_{N_e/2+1} \leqslant \cdots \leqslant \epsilon_{N_b}. \tag{20}$$

Then, $\epsilon_{N_e/2}$ and $\epsilon_{N_e/2+1}$ are the HOMO and LUMO energies, respectively. The product of ρ and H can be easily found:

$$\rho H = H\rho = \mathrm{diag}(\epsilon_1, \epsilon_2, \ldots, \epsilon_{N_e/2}, 0, \ldots, 0) \tag{21}$$

and we can shift the Hamiltonian H to $H + \lambda I (\lambda > 0)$ so that $\lambda + \epsilon_{N_e/2} > 0$, and $\lambda + \epsilon_{N_e/2}$ is the largest eigenvalue of $\rho(H + \lambda I)$. The parameter λ can be set to a large positive value, and in practice, it is usually reliable to set it as 1.0 Ry. The largest eigenvalue and its corresponding eigenvector of $\rho(H + \lambda I)$ can be computed easily using the $O(N)$ Lanczos method. A similar approach can also be applied for LUMO [31].

The scheme described above is for the orthogonal basis, and can be illustrated in Figure 7(a). If an NAO basis set is used, the non-orthogonal basis set should generally be first convert to an orthogonal basis set using Cholesky decomposition or the Löwdin decomposition of the overlap matrix S.

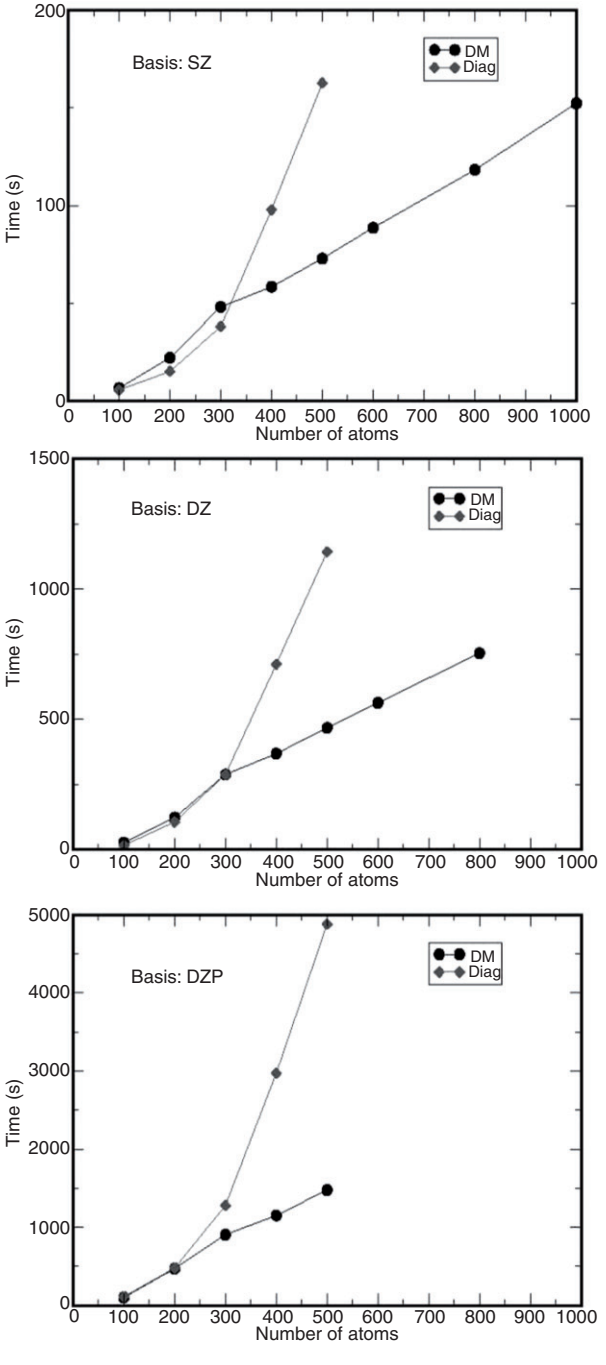

Figure 6. CPU time per SCF cycle for a carbon-doped BN(5, 5) nanotube using the PSUTC2 method and the traditional diagonalization method with different basis sets. (Reproduced with permission from ref. [28]. Copyright 2005 American Institute of Physics.)

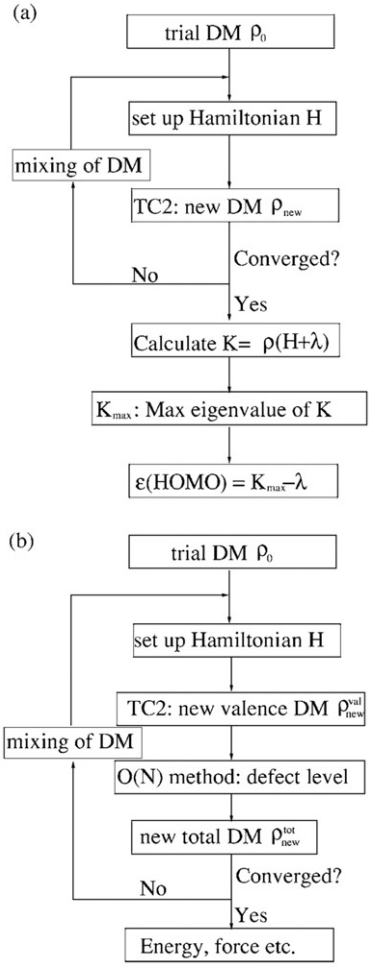

Figure 7. Schematic illustration of (a) the $O(N)$ method for calculating the HOMO state. The program flow for the LUMO calculation is similar. (b) The $O(N)$ method for dealing with doped semiconductors. Here 'density matrix' is abbreviated to 'DM'. (Reproduced with permission from ref. [31]. Copyright 2007 American Institute of Physics.)

It is also possible to calculate the band edge state in a non-orthogonal basis without transforming to an orthogonal basis. We use the suffix 'ao' for non-orthogonal atomic orbital basis sets. As $\rho_{\mathrm{ao}}(H_{\mathrm{ao}}+\lambda IS)$ have the same eigenvalues as $\rho(H+\lambda I)$, the largest eigenvalue of $\rho_{\mathrm{ao}}(H_{\mathrm{ao}}+\lambda IS)$ will be $\epsilon_{\mathrm{HOMO}}+\lambda$.

Based on the scheme described above, we have further developed an $O(N)$ algorithm to deal with doped semiconductors (illustrated in Figure 7b). In each cycle, the valence band and the doping state are calculated respectively. The valence band density matrix is obtained using traditional $O(N)$ methods, such as TC2. Other defective bands are calculated using the $O(N)$ method band edge states as mentioned above.

This $O(N)$ method for doped semiconductors has been used to treat large-radius BN nanotubes with an isolated adsorbed H atom using huge supercells. Three BN nanotubes

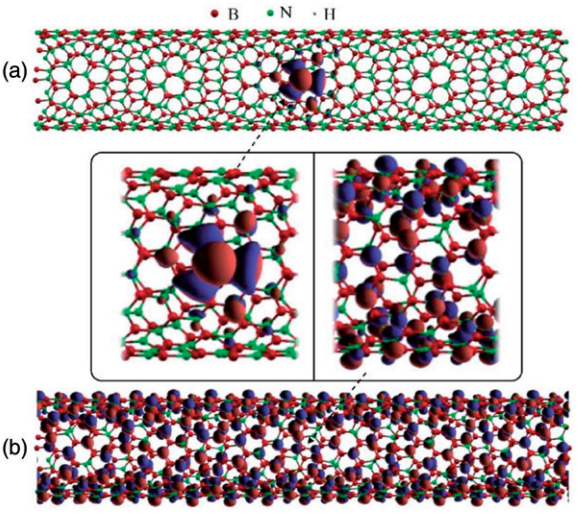

Figure 8. (a) The acceptor state and (b) the highest orbital of the valence band of a BN(13, 2) nanotube with an isolated adsorbed H atom. The insets show the enlarged plots around the adsorbed H atom. (Reproduced with permission from ref. [31]. Copyright 2007 American Institute of Physics.)

are considered: a BN(8, 0) nanotube simulated using a supercell with 320 atoms, a BN(15, 0) nanotube simulated using a supercell with 720 atoms, and a BN(13, 2) nanotube with 796 atoms in the unit cell. The distribution of the acceptor state and the highest orbital of the valence band are shown in Figure 8. Clearly, the acceptor state is a relatively localized state around the adsorbed H atom, which agrees with the result reported by Wu *et al*. [110,111]. However, the highest orbital of the valence band is delocalized and mainly contributed by $N\ 2p_z$ orbitals. The calculated acceptor levels (i.e. the energy difference between the acceptor state and the top of the valence band) introduced by an isolated H atom are 1.184, 1.557, and 1.563 eV for BN(8, 0), BN(15, 0), and BN(13, 2) nanotubes, respectively. Thus the position of the defect level is closer to the top of valence bands for smaller-radius BN nanotubes, but does not depend significantly on the chirality.

5.2. *Maximally localized Wannier functions*

Wannier functions [112] are a kind of local orbitals, and are very useful in the study of chemical bonding, dielectric properties, excited electronic states, electron transport, and many-body correlations in materials. Marzari and Vanderbilt have proposed a method [113] to obtain a unique set of MLWFs. Using MLWFs, we can get an enhanced understanding of chemical bonding properties and electric polarization. We can also use the MLWFs as a minimal basis for a variety of purposes, such as linear scaling calculations [114], construction of effective Hamiltonians for the study of ballistic transport [115,116], strongly correlated electrons [117–119], self-interaction corrections, metal–insulator transitions [120], and photonic lattices [121].

After the self-consistent ground state calculation, we found that the MLWFs can be calculated with the numerical atomic orbital basis in a linear scaling way by three $O(N)$ steps [29]. First, using the density matrix obtained above, we can find a set of linearly

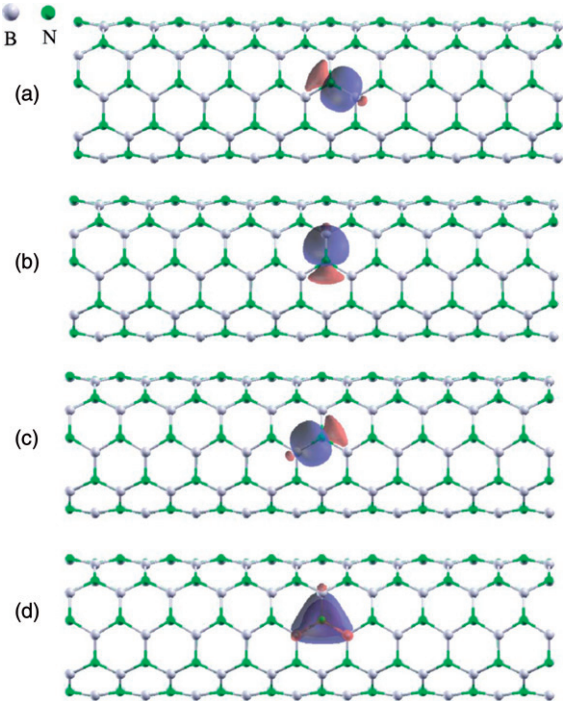

Figure 9. [Colour online] Four MLWFs around a nitrogen atom of BN(5, 5) nanotubes. These MLWFs are calculated using the supercell containing 200 atoms with the DZP basis set. (Reproduced with permission from ref. [29]. Copyright 2006 American Institute of Physics.)

independent non-orthogonal orbitals which span the occupied manifold,

$$\Phi_\alpha = \rho|\varphi_\alpha\rangle = \sum_\beta (\rho S)_{\beta,\alpha}|\varphi_\beta\rangle \tag{22}$$

where ρ and S denote the density matrix and overlap matrix, respectively, and φ_α and φ_β are atomic orbitals. Second, a modified Löwdin orthogonalization is used to orthogonalize these non-orthogonal orbitals. Finally, the Jacobi rotation scheme is utilized to maximally localize the orbitals.

The method has been applied to calculate the MLWFs of a BN(5, 5) armchair nanotube. Figure 9 shows four MLWFs of the BN(5, 5) nanotube computed using a supercell containing 200 atoms. Two different basis sets, SZ and DZP, are employed in the calculations using the new $O(N)$ method, and only the SZ basis set is used for the traditional method. The CPU time is shown in Figure 10. We clearly see the perfect linear scaling behaviour of this new method, and the traditional method displays a nearly $O(N^3)$ scaling as expected. The computing saving of this method with respect to the traditional method is dramatically large, especially when the size of systems exceeds 400 atoms.

6. Response theory

Response theory is used to compute both dynamic and static response properties. The former can be computed by propagating the density matrix in the time domain [122,123],

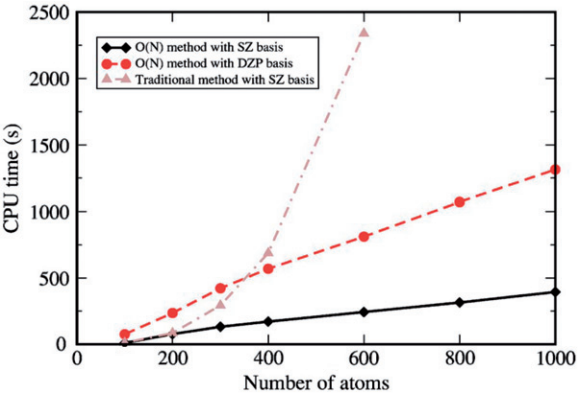

Figure 10. [Colour online] Total CPU time for calculating MLWFs of a BN(5, 5) nanotube using the linear scaling method or the traditional Jacobi rotation method which does not take advantage of the localization property of the orbitals. In the case of the new $O(N)$ method, both SZ and DZP basis sets are used. The calculations using the traditional method are performed using the SZ basis set. (Reproduced with permission from ref. [29]. Copyright 2006 American Institute of Physics.)

and then performing a convolution to obtain the spectral response. The static response properties, such as, the polarizability, nuclear magnetic resonance, Raman intensities, vibrational frequencies, and the magnetic susceptibility [124,125], are conventionally obtained by solving the coupled-perturbed self-consistent-field (CPSCF) equations. Several algorithms have been proposed for solving the CPSCF equations that may be capable of achieving $O(N)$ scaling [126,127] by avoiding both eigenproblem solution and integral transformation. But these methods only give an implicit solution of the CPSCF equation [125]. On the other hand, the $O(N)$ density-matrix perturbation theory (DMPT) [34] method provides explicit construction of the derivative density matrix. TC2 purification provides a possible recursive way to construct the derivative density matrix.

6.1. *Density-matrix perturbation theory*

To get the response properties, we need to calculate the density matrix derivatives with respect to a perturbation. We assume a perturbation expansion of the Hamiltonian H [128]:

$$H = H^{(0)} + \lambda H^{(1)} + \lambda^2 H^{(2)} + \cdots. \tag{23}$$

This generates the corresponding density matrix perturbed sequence in its intermediates form $X_n^{(m)}$:

$$X_n = X_n^{(0)} + \lambda X_n^{(1)} + \lambda^2 X_n^{(2)} + \cdots \tag{24}$$

where the mth-order $X_n^{(m)}$ can be found in the following way:

$$X_{n+1}^{(m)} = \begin{cases} \sum_{i=0}^{m} X_n^{(i)} X_n^{(m-i)} & \mathrm{Tr}(X_n^{(0)}) \geq N \\ 2X_n^{(m)} - \sum_{i=0}^{m} X_n^{(i)} X_n^{(m-i)} & \mathrm{Tr}(X_n^{(0)}) < N. \end{cases} \tag{25}$$

Then the mth-order density matrix derivatives are given by

$$\rho^{(m)} = \lim_{n\to\infty} X_n^{(m)} \tag{26}$$

and corresponding density matrix is

$$\rho = \rho^{(0)} + \lambda\rho^{(1)} + \lambda^2\rho^{(2)} + \cdots. \tag{27}$$

The initial matrices $X_0^{(0)}$ and $X_0^{(m)}$ are computed as

$$X_0^{(0)} = \frac{\epsilon_{\max} - H^{(0)}}{\epsilon_{\max} - \epsilon_{\min}} \tag{28}$$

$$X_0^{(m)} = \frac{-H^{(m)}}{\epsilon_{\max} - \epsilon_{\min}} \tag{29}$$

where $\epsilon_{\max}$ and $\epsilon_{\min}$ are the maximal and minimal eigenvalues of the unperturbed Hamiltonian $H^{(0)}$, respectively.

For example, to first order, the DMPT equations are:

$$X_{n+1}^{(1)} = \begin{cases} X_n^{(1)}X_n^{(0)} + X_n^{(0)}X_n^{(1)} & \mathrm{Tr}(X_n^{(0)}) \geq N \\ 2X_n^{(1)} - X_n^{(1)}X_n^{(0)} - X_n^{(0)}X_n^{(1)} & \mathrm{Tr}(X_n^{(0)}) < N \end{cases} \tag{30}$$

where the $X_n^{(0)}$ is found in the following cycle:

$$X_{n+1}^{(0)} = \begin{cases} (X_n^{(0)})^2 & \mathrm{Tr}(X_n^{(0)}) \geq N \\ 2X_n^{(0)} - (X_n^{(0)})^2 & \mathrm{Tr}(X_n^{(0)}) < N. \end{cases} \tag{31}$$

These equations provide the base for computing the density-matrix response explicitly and rapidly. This orthogonal form can be generalized to non-orthogonal form by including basis-set-dependent perturbations [128]. The DMPT method has been used for the computation of the high-frequency molecular dielectric tensor [125] and response properties beyond second order [129] based on GTOs.

6.2. *Electric field perturbation in solids by DMPT*

It is well known that a uniform electric field in periodic systems is notably difficult to treat since the position operator is ill-defined in periodic boundary conditions. We proposed a method to address this issue using the DMPT approach [30]. First, we discovered that $\rho^{(1)}$ is only determined by the sum of the non-diagonal parts of the first-order derivative Hamiltonian matrix, i.e.

$$H^{(0)}\rho^{(1)} - \rho^{(1)}H^{(0)} = \rho^{(0)}H_{\mathrm{nd}}^{(1)} - H_{\mathrm{nd}}^{(1)}\rho^{(0)} \tag{32}$$

where $H_{\mathrm{nd}}^{(1)} = H_{\mathrm{VC}}^{(1)} + H_{\mathrm{CV}}^{(1)}$ is the non-diagonal part of the first-order derivative Hamiltonian matrix, and they are computed by the projector operators P_{V} and P_{C}:

$$P_{\mathrm{V}} = \rho^{(0)}, \quad P_{\mathrm{C}} = I - \rho^{(0)} \tag{33}$$

$$H_{\mathrm{VC}}^{(1)} = P_{\mathrm{V}}H^{(1)}P_{\mathrm{C}}, \quad H_{\mathrm{CV}}^{(1)} = P_{\mathrm{C}}H^{(1)}P_{\mathrm{V}} \tag{34}$$

where $\rho^{(0)}$ is the zero-order ground state orthogonal density matrix.

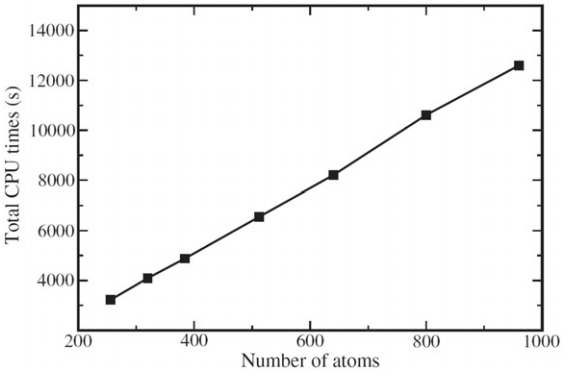

Figure 11. Total CPU time for computing the polarizability of a BN (8, 0) nanotube using the $O(N)$ DMPT method. The electric field is along the axis direction. (Reproduced with permission from ref. [30]. Copyright 2006 American Physical Society.)

For electric field ϵ along the β direction, $H^{(1)} = er_\beta + \partial V^{\mathrm{Hxc}}/\partial\epsilon_\beta$, and $H^{(1)}_{\mathrm{nd}}$ is well-defined since $P_{\mathrm{C}} r_\beta P_{\mathrm{V}} + P_{\mathrm{V}} r_\beta P_{\mathrm{C}} = [r_\beta, \rho^{(0)}]\rho^{(0)} + \rho^{(0)}[\rho^{(0)}, r_\beta]$, and $[\rho^{(0)}, r_\beta]$ is well-defined. As a result, $H^{(1)}_{\mathrm{nd}}$ instead of $H^{(1)}$ is used as the perturbation operator in DMPT. When $\rho^{(1)}$ is obtained using Equation (30), we can get the first-order variation of the electric polarizability:

$$\frac{\partial P_\alpha}{\partial \epsilon_\beta} = -\frac{2e}{\Omega_0}\mathrm{Tr}(\rho^{(1)} r_\alpha); \tag{35}$$

the factor of 2 is from spin degeneracy, and Ω_0 is the unit-cell volume.

The polarizability of a BN(8, 0) nanotube has been calculated using the $O(N)$ DMPT method. The CPU time is shown in Figure 11, which clearly shows perfect linear-scaling behaviour.

The Born effective charge is defined as the change in macroscopic polarization P_β along the direction β upon the collective nuclear displacements of atoms I along direction α under the condition of zero macroscopic electric field, times the unit-cell volume Ω_0:

$$Z_{I,\alpha\beta} = \Omega_0 \left.\frac{\partial P_\beta}{\partial R_{I,\alpha}}\right|_{\epsilon=0}. \tag{36}$$

Using the traditional Clausius–Mossotti (CM) relation, $\partial P/\partial R_I$ can be calculated as:

$$\frac{\partial P}{\partial R_I} = -\frac{e}{\Omega_0} \times \int \mathbf{r}\frac{\partial n(\mathbf{r})}{\partial R_I}\,\mathrm{d}\mathbf{r} \tag{37}$$

where n is the electronic density. For molecular orbital ψ_i and atomic basis function ϕ_μ, we have

$$n = 2\sum_i^{\mathrm{occ}} \psi_i \psi_i \tag{38}$$

$$\psi_i = \sum_\mu c_{\mu i}\phi_\mu. \tag{39}$$

Using the above equations, we get:

$$\frac{\partial n}{\partial R_I} = \sum_{\mu\nu} \left(4\rho_{\mu\nu}\phi_\nu \frac{\partial \phi_\mu}{\partial R_I} + 2\frac{\partial \rho_{\mu\nu}}{\partial R_I}\phi_\mu\phi_\nu \right) \tag{40}$$

where $\rho_{\mu\nu}$ is a density matrix element:

$$\rho_{\mu\nu} = \sum_{i}^{\text{occ}} c_{\mu i} c_{\nu i}. \tag{41}$$

As a result, when $\partial\rho_{\mu\nu}/\partial R_I$ is calculated by DMPT, we can get the Born effective charge using Equation (36).

We note that the CM method for calculating the difference of electronic polarization between two states is useful for large systems, although it does not work well for systems with small unit cells where one may resort to the Berry-phase method [130,131]. Amorphous SiO_2 with a realistic 648-atom model generated by Tafen and Drabold [132,133] has been studied. The calculated average isotropic Born charge for Si is 3.29, which is a little larger than that for a 72-atom model (3.18) [134].

7. Conclusions and outlook

In this review, we have described the $O(N)$ algorithms ranging from ground state calculations to response properties with NAO basis sets. Two kinds of representative NAO construction methods have been introduced. Both methods lead to strictly truncated NAOs by applying confining potentials. Based on the locality of NAOs, the Hamiltonian and density matrix will be sparse, which provides a possibility for linear scaling.

The strong demand of linear scaling methods comes from a various fields, especially nanomaterials and biochemistry. For nano- and biosystems, calculation of the total energy, optimization of the structure, and analysis of the electronic properties usually need to be handled using $O(N)$ approaches [91]. With stable linear scaling methods, computational characterization of complex systems and theoretical design of new functional materials will play a more and more important role in modern physical sciences.

Many $O(N)$ algorithms have been implemented based on NAOs, especially with purification approaches. However, there is still much room for improving these methods in terms of efficiency as well as accuracy. For example, the current available $O(N)$ algorithms for metallic systems are inefficient. In addition, conventional DFT theory suffers from the self-interaction problem, and hybrid functionals [61,135] that mixes some exact exchange counteract this effect. HFX can also serve as a starting point for the implementation of MP2 and other correlated methods for large systems [136–146]. Therefore, efficient HFX calculations are strongly pursued in the DFT community using NAO basis sets. However, calculating HFX with NAO basis sets is still very time consuming [17,18,67]. Better algorithms which provide a good balance between accuracy and efficiency are urgently needed.

Acknowledgements

This work is partially supported by NSFC (50721091, 20873129, and 20933006) and by the National Key Basic Research Program (2006CB922004).

References

[1] R. G. Parr and W. Yang, *Density Functional Theory of Atoms and Molecules* (Oxford University Press, New York, 1989).
[2] P. Hohenberg and W. Kohn, Phys. Rev. B **136**, 864 (1964).
[3] W. Kohn and L. Sham, Phys. Rev. **140**, 1133 (1965).
[4] A. Szabo and N. S. Ostlund, *Modern Quantum Chemistry – Introduction to Advanced Electronic Structure Theory* (McGraw-Hill, New York, 1989).
[5] S. Goedecker, Rev. Mod. Phys. **71**, 1085 (1999).
[6] W. Kohn, Int. J. Quart. Chem. **56**, 229 (1995).
[7] W. Kohn, Phys. Rev. Lett. **76**, 3168 (1996).
[8] J. M. Soler, E. Artacho, J. D. Gale, A. Garcia, J. Junquera, P. Ordejón, and D. Sánchez-Portal, J. Phys. Condens. Matter. **14**, 2745 (2002).
[9] O. Sankey and D. Niklewski, Phys. Rev. B **40**, 3979 (1989).
[10] F. Averill and D. Ellis, J. Chem. Phys. **59**, 6412 (1973).
[11] A. Zunger and A. Freeman, Phys. Rev. B **15**, 4716 (1977).
[12] B. Delley and D. Ellis, J. Chem. Phys. **76**, 1949 (1982).
[13] S. D. Kenny, A. P. Horsfield, and H. Fujitani, Phys. Rev. B **62**, 4899 (2000).
[14] G. te Velde, F. Bickelhaupt, E. Baerends, C. F. Guerra, S. van Gisbergen, J. Snijders, and T. Ziegler, J. Comput. Chem. **22**, 931 (2001).
[15] K. Koepernik and H. Eschrig, Phys. Rev. B **59**, 1743 (1999).
[16] A. Horsfield, Phys. Rev. B **56**, 6594 (1991).
[17] T. Ozaki, H. Kino, J. Yu, M. Han, N. Kobayashi, M. Ohfuti, F. Ishii, and T. Ohwaki, User's Manual of OpenMX; http://www.openmx-square.org (2008).
[18] V. Blum, R. Gehrke, F. Hanke, P. Havu, V. Havu, X. Ren, K. Reuter, and M. Scheffler, The Fritz Haber Institute *ab initio* molecular simulations package (FHI-aims); http://www.fhi-berlin.mpg.de/aims (2009).
[19] B. Delley, J. Chem. Phys. **92**, 508 (1990).
[20] J. Talman, J. Chem. Phys. **80**, 2000 (1984).
[21] J. Talman, J. Chem. Phys. **84**, 6879 (1986).
[22] J. Talman, Int. J. Quantum Chem. **93**, 72 (2003).
[23] J. Talman, Int. J. Quantum Chem. **95**, 442 (2003).
[24] J. Talman, Collect. Czech. Chem. Commun. **70**, 1035 (2005).
[25] J. Talman, Int. J. Quantum Chem. **107**, 1578 (2007).
[26] J. Talman, Phys. Rev. Lett. **84**, 855 (2000).
[27] A. S. Torralba, M. Todorovic, V. Brazdova, R. Choudhury, T. Miyazaki, M. J. Gillan, and D. R. Bowler, J. Phys.: Condens. Matter **20**, 294206 (2008).
[28] H. J. Xiang, W. Z. Liang, J. L. Yang, J. G. Hou, and Q. S. Zhu, J. Chem. Phys. **123**, 124105 (2005).
[29] H. J. Xiang, Z. Y. Li, W. Z. Liang, J. L. Yang, J. G. Hou, and Q. S. Zhu, J. Chem. Phys. **124**, 234108 (2006).
[30] H. J. Xiang, J. L. Yang, J. G. Hou, and Q. S. Zhu, Phys. Rev. Lett. **97**, 266402 (2006).
[31] H. J. Xiang, J. L. Yang, J. G. Hou, and Q. S. Zhu, J. Chem. Phys. **126**, 244707 (2007).
[32] T. Ozaki, Phys. Rev. B **67**, 155108 (2003).
[33] V. Blum, R. Gehrke, F. Hanke, P. Havu, V. Havu, X. Ren, K. Reuter, and M. Scheffler, Comput. Phys. Commun. **180**, 2175 (2009).
[34] A. M.N. Niklasson and M. Challacombe, Phys. Rev. Lett. **92**, 193001 (2004).
[35] C. Froese Fischer, *The Hartree–Fock Method for Atoms: A Numerical Approach* (Wiley Interscience, New York, 1977).
[36] S. F. Boys, Proc. R. Soc. London, Ser. A **200**, 542 (1950).

[37] S. F. Boys, Proc. R. Soc. London, Ser. A **201**, 125 (1950).
[38] S. F. Boys, Proc. R. Soc. London, Ser. A **258**, 402 (1960).
[39] W. J. Hehre, I. Radom, P. V. R. Schleyer, and J. A. Pople, *Ab Initio Molecular Orbital Theory* (John Wiley, New York, 1986).
[40] S. Huzinaga, *Gaussian Basis Sets for Molecular Calculations* (Elsevier, Amsterdam, 1984).
[41] T. H. Dunning Jr and P. J. Hay, in *Methods of Electronic Structure Theory*, edited by H. F. Schaefer III (Plenum, New York, 1977), p. 1.
[42] E. Artacho, D. Sánchez-Portal, P. Ordejón, A. García, and J.M. Soler, Phys. Status Solidi B **215**, 809 (1999).
[43] J. Junquera, Ó. Paz, D. Sánchez-Portal, and E. Artacho, Phys. Rev. B **64**, 235111 (2001).
[44] T. Ozaki and H. Kino, Phys. Rev. B **69**, 195113 (2004).
[45] T. Ozaki and H. Kino, J. Chem. Phys. **121**, 10879 (2004).
[46] B. Delley, J. Chem. Phys. **113**, 7756 (2000).
[47] E. Anglada, J. M. Soler, J. Junquera, and E. Artacho, Phys. Rev. B **66**, 205101 (2002).
[48] V. Havu, V. Blum, P. Havu, and M. Scheffler, J. Comput. Phys. **228**, 8367 (2009).
[49] D. Porezag, T. Frauenheim, T. Köhler, G. Seifert, and R. Kaschner, Phys. Rev. B **51**, 12947 (1995).
[50] A. P. Horsfield, Phys. Rev. B **56**, 6594 (1997).
[51] J. Almlöf, K. Faegri Jr, and K. Korsell, J. Comput. Chem. **3**, 385 (1982).
[52] D. Cremer and J. Gauss, J. Comput. Chem. **7**, 274 (1986).
[53] M. Häser and R. Ahlrichs, J. Comput. Chem. **10**, 104 (1989).
[54] C. Ochsenfeld, C. A. White, and M. Head-Gordon, J. Chem. Phys. **109**, 1663 (1998).
[55] C. A. White and M. Head-Gordon, Chem. Phys. Lett. **230**, 8 (1994).
[56] C. A. White, B. G. Johnson, P. M.W. Gill, and M. Head-Gordon, Chem. Phys. Lett. **253**, 268 (1996), and references therein.
[57] C. A. White and M. Head-Gordon, J. Chem. Phys. **105**, 5061 (1996).
[58] M. C. Strain, G. E. Scuseria, and M. J. Frisch, Science **271**, 51 (1996).
[59] M. Challacombe, E. Schwegler, and J. Almlöf, J. Chem. Phys. **104**, 4685 (1996).
[60] M. Challacombe and E. Schwegler, J. Chem. Phys. **106**, 5526 (1997).
[61] A. D. Becke, J. Chem. Phys. **98**, 5648 (1993).
[62] E. Schwegler and M. Challacombe, J. Chem. Phys. **105**, 2726 (1996).
[63] J. C. Burant, G. E. Scuseria, and M. J. Frisch, J. Chem. Phys. **105**, 8969 (1996).
[64] E. Schwegler, M. Challacombe, and M. Head-Gordon, J. Chem. Phys. **106**, 9708 (1997).
[65] X. Wu, A. Selloni, and R. Car, Phys. Rev. B **79**, 085102 (2009).
[66] M. Toyoda and T. Ozaki, J. Chem. Phys. **130**, 124114 (2009).
[67] H. H. Shang, Z. Y. Li, and J. L. Yang, J. Phys. Chem. A **114**, 1039 (2010).
[68] L. Kleinman and D. Bylander, Phys. Rev. Lett. **48**, 1425 (1982).
[69] P. Mori-Sanchez, A. J. Cohen, and W. Yang, Phys. Rev. Lett. **100**, 146401 (2008).
[70] L. Genovese, T. Deutsch, A. Neelov, S. Goedecker, and G. Beylkin, J. Chem. Phys. **125**, 074105 (2006).
[71] W. Yang, Phys. Rev. Lett. **66**, 1438 (1991).
[72] A. M. N. Niklasson, C. J. Tymczak, and M. Challacombe, J. Chem. Phys. **118**, 8611 (2003).
[73] A. M. N. Niklasson, Phys. Rev. B **66**, 155115 (2002).
[74] A. D. Daniels and G. E. Scuseria, J. Chem. Phys. **110**, 1321 (1999).
[75] S. L. Dixon and K. M. Merz, J. Chem. Phys. **104**, 6643 (1996).
[76] S. L. Dixon and K. M. Merz, J. Chem. Phys. **107**, 879 (1997).
[77] S. Goedecker and L. Colombo, Phys. Rev. Lett. **73**, 122 (1994).
[78] S. Goedecker and M. Teter, Phys. Rev. B **51**, 9455 (1995).
[79] W. Z. Liang, C. Saravanan, Y.H. Shao, R. Baer, A.T. Bell, and M. Head-Gordon, J. Chem. Phys. **119**, 4117 (2003).
[80] A. F. Voter, J. D. Kress, and R. N. Silver, Phys. Rev. B **53**, 12733 (1996).

[81] X.-P. Li, R. W. Nunes, and D. Vanderbilt, Phys. Rev. B **47**, 10891 (1993).
[82] M. S. Daw, Phys. Rev. B **47**, 10895 (1993).
[83] R. W. Nunes and D. Vanderbilt, Phys. Rev. B **50**, 17611 (1994).
[84] P. D. Haynes and M. C. Payne, Phys. Rev. B **59**, 12173 (1999).
[85] F. Mauri, G. Galli, and R. Car, Phys. Rev. B **47**, 9973 (1993).
[86] J. Kim, F. Mauri, and G. Galli, Phys. Rev. B **52**, 1640 (1995).
[87] P. Ordejón, D. Drabold, M. Grumbach, and R. M. Martin, Phys. Rev. B **48**, 14646 (1993).
[88] L.-W. Wang and M. Teter, Phys. Rev. B **44**, 12798 (1992).
[89] W. Yang, Phys. Rev. B **56**, 9294 (1997).
[90] R. McWeeny, Rev. Mod. Phys. **32**, 335 (1960).
[91] D. R. Bowler and T. Miyazaki, J. Phys. Condens. Matter. **22**, 074207 (2010).
[92] E. Hernández and M. J. Gillan, Phys. Rev. B **51**, 10157 (1995).
[93] C. M. Goringe, E. Hernández, M. J. Gillan, and I. J. Bush, Comput. Phys. Commun. **102**, 1 (1997).
[94] E. Hernández, M. Gillan, and C. Goringe, Phys. Rev. B **53**, 7147 (1996).
[95] D. R. Bowler and M. J. Gillan, Comput. Phys. Commun. **120**, 95 (1999).
[96] D. R. Bowler, I. J. Bush, and M. J. Gillan, Int. J. Quantum Chem. **77**, 831 (2000).
[97] D. R. Bowler, T. Miyazaki, and M. J. Gillan, J. Phys.: Condens. Matter **14**, 2781 (2002).
[98] T. Miyazaki, D. R. Bowler, R. Choudhury, and M. J. Gillan, J. Chem. Phys. **121**, 6186 (2004).
[99] D. R. Bowler, R. Choudhury, M. J. Gillan, and T. Miyazaki, Phys. Status Solidi b **243**, 989 (2006).
[100] D. R. Bowler, T. Miyazaki, and M. J. Gillan, Comput. Phys. Commun. **137**, 255 (2001).
[101] P. Ordejón, D. A. Drabold, M. P. Grumbach, and R. M. Martin, Phys. Rev. B **51**, 1456 (1995).
[102] A. H. R. Palser and D. E. Manolopoulos, Phys. Rev. B **58**, 12704 (1998).
[103] S. Y. Wu and C. S. Jayanthi, Phys. Rep. **358**, 1 (2002).
[104] A. M. N. Niklasson, C. J. Tymczak, and H. Roder, Phys. Rev. B **66**, 155120 (2002).
[105] C. Saravanan, Y. Shao, R. Baer, P. N. Ross, and M. Head-Gordon, J. Comput. Chem. **24**, 618 (2003).
[106] M. Challacombe, J. Chem. Phys. **110**, 2332 (1999).
[107] M. Challacombe, Comput. Phys. Commun. **128**, 93 (2000).
[108] R. Q. Wu, L. Liu, G. W. Peng, and Y. P. Feng, Appl. Phys. Lett. **86**, 122510 (2005).
[109] V. Bach, E. H. Lieb, M. Loss, and J. P. Solovej, Phys. Rev. Lett. **72**, 2981 (1994).
[110] X. J. Wu, J. L. Yang, J. G. Hou, and Q. S. Zhu, Phys. Rev. B **69**, 153411 (2004).
[111] X. J. Wu, J. L. Yang, J. G. Hou, and Q. S. Zhu, J. Chem. Phys. **121**, 8481 (2004).
[112] G. H. Wannier, Phys. Rev. **52**, 191 (1937).
[113] N. Marzari and D. Vanderbilt, Phys. Rev. B **56**, 12847 (1997).
[114] A. J. Williamson, R. Q. Hood, and J. C. Grossman, Phys. Rev. Lett. **87**, 246406 (2001).
[115] A. Calzolari, N. Marzari, I. Souza, and M. B. Nardelli, Phys. Rev. B **69**, 035108 (2004).
[116] Z. Li and D. S. Kosov, J. Phys.: Condens. Matter **18**, 1347 (2006).
[117] W. Ku, H. Rosner, W. E. Pickett, and R. T. Scalettar, Phys. Rev. Lett. **89**, 167204 (2002).
[118] I. Schnell, G. Czycholl, and R. C. Albers, Phys. Rev. B **65**, 075103 (2002).
[119] K. Nakamura, R. Arita, Y. Yoshimoto and S. Tsuneyuki, cond-mat/0510425.
[120] E. Pavarini, S. Biermann, A. Poteryaev, A. I. Lichtenstein, A. Georges, and O. K. Andersen, Phys. Rev. Lett. **92**, 176403 (2004).
[121] D. M. Whittaker and M. P. Croucher, Phys. Rev. B **67**, 085204 (2003).
[122] S. Nomura, T. Iitaka, X. W. Zhao, T. Sugano, and Y. Aoyagi, Phys. Rev. B **56**, 4348 (1997).
[123] C. Y. Yam, S. Yokojima, and G. H. Chen, Phys. Rev. B **68**, 153105 (2003).
[124] J. Autschbach and T. Ziegler, Coord. Chem. Rev. **238**, 83 (2003).
[125] V. Weber, A. M. N. Niklasson, and M. Challacombe, Phys. Rev. Lett. **92**, 193002 (2004).
[126] C. Ochsenfeld and M. Head-Gordon, Chem. Phys. Lett. **270**, 399 (1997).
[127] W. Z. Liang, Y. Zhao, and M. Head-Gordon, J. Chem. Phys. **123**, 194106 (2005).

[128] A. M. N. Niklasson, V. Weber, and M. Challacombe, J. Chem. Phys. **123**, 044107 (2005).
[129] V. Weber, A. M. N. Niklasson, and M. Challacombe, J. Chem. Phys. **123**, 044106 (2005).
[130] R. D. King-Smith and D. Vanderbilt, Phys. Rev. B **47**, 1651 (1993).
[131] R. Resta, Rev. Mod. Phys. **66**, 899 (1994).
[132] D. N. Tafen and D. A. Drabold, Phys. Rev. B **71**, 054206 (2005).
[133] D. N. Tafen and D. A. Drabold, Phys. Rev. B **68**, 165208 (2003).
[134] A. Pasquarello and R. Car, Phys. Rev. Lett. **79**, 1766 (1997).
[135] J. Heyd, G. E. Scuseria, and M. Ernzerhof, J. Chem. Phys. **118**, 8207 (2003).
[136] M. Marsman, A. Grüneis, J. Paier, and G. Kresse, J. Chem. Phys. **130**, 184103 (2009).
[137] A. Grüneis, M. Marsman, and G. Kresse, J. Chem. Phys. **133**, 074107 (2010).
[138] C. Pisani, M. Busso, G. Capecchi, S. Casassa, R. Dovesi, L. Maschio, C. Zicovich-Wilson, and M. Schütz, J. Chem. Phys. **122**, 094113 (2005).
[139] S. Casassa, M. Halo, L. Maschio, C. Roetti, and C. Pisani, Theor. Chem. Acc. **117**, 781 (2007).
[140] C. Pisani, L. Maschio, S. Casassa, M. Halo, Schütz, and D. Usvyat, J. Comput. Chem. **29**, 2113 (2008).
[141] F. R. Manby, D. Almlöf, and M. J. Gillan, Phys. Chem. Chem. Phys. **8**, 5178 (2006).
[142] S. J. Nolan, M. J. Gillan, D. Almlöf, N. L. Allan, and F. R. Manby, Phys. Rev. B **80**, 165109 (2009).
[143] P. Y. Ayala, K. N. Kudin, and G. E. Scuseria, J. Chem. Phys. **115**, 9698 (2001).
[144] J.-Q. Sun and R. J. Bartlett, J. Chem. Phys. **104**, 8553 (1996).
[145] S. Hirata, R. Podeszwa, M. Tobita, and R. J. Bartlett, J. Chem. Phys. **120**, 2581 (2004).
[146] B. Doser, D. S. Lambrecht, J. Kussmann, and C. Ochsenfeld, J. Chem. Phys. **130**, 064107 (2009).